The Astrophysical Journal, 504:900–914, 1998 September 10

L1544: A STARLESS DENSE CORE WITH EXTENDED INWARD MOTIONS

M. Tafalla,[1] D. Mardones, and P. C. Myers
Harvard-Smithsonian Center for Astrophysics, MS 42, 60 Garden Street, Cambridge, MA 02138; tafalla@oan.es, dmardones@cfa.harvard.edu, pmyers@cfa.harvard.edu
P. Caselli
Osservatorio Astrofisico di Arcetri, Largo Enrico Fermi 5, I-50125 Firenze, Italy
R. Bachiller
Observatorio Astronómico Nacional, Campus Universitario, Apartado 1143, E-28800, Alcalá de Henares, Madrid, Spain; bachiller@cay.es
and
P. J. Benson
Whitin Observatory, Wellesley College, 106 Central Street, Wellesley, MA 02181
Received 1997 December 30; accepted 1998 April 14

ABSTRACT

We present a multiline study of the dense core L1544 in the Taurus molecular complex. Although L1544 does not harbor an embedded star, it presents several characteristics of cores that have already undergone star formation, suggesting that it may be rather advanced in its evolution toward becoming a star-forming core. The spectral lines from L1544 present an interesting dichotomy, with the thick dense gas tracers suffering very strong self absorption while CO and its isotopes are not being absorbed at all. The presence of the self absorptions allows us to study both the density structure and kinematics of the gas in detail. A simple analysis shows that the core is almost isothermal and that the self absorptions are due to very subthermal excitation of the dense gas tracers in the outer layers. The density has to decrease outward rapidly, and a detailed radiative transfer calculation that simultaneously fits three isotopes of CO and two of CS shows that the density approximately follows a $r^{-1.5}$ power law. The self absorptions, in addition, allow us to measure the relative velocity between the inner and outer layers of the core, and we find that there is a global pattern of inward motions (background and foreground approaching each other). The relative speed between the foreground and background changes with position, and we use a simple two-layer model to deduce that while the foreground gas has a constant velocity, the background material presents systematic velocity changes that we interpret as arising from two velocity components. We explore the origin of the inward motions by comparing our observations with models of gravitational collapse. A model in which the infall starts at the center and propagates outward (as in the inside-out collapse of Shu) is inconsistent with the large extension of the absorption (that suggests an advanced age) and the lack of a star at the core center (that suggests extreme youth). Ambipolar diffusion seems also ruled out because of the large amount of the inward speed (up to 0.1 km s^{-1}) and the fact that ionized species move with speeds similar to those of the neutrals. Other infall models seem also to have problems fitting the data, so if L1544 is infalling, it seems to be doing so in a manner not contemplated by the standard theories of star formation. Our study of L1544 illustrates how little is still known about the physical conditions that precede star formation and how detailed studies of starless cores are urgently needed.

Subject headings: ISM: individual (L1544) — ISM: kinematics and dynamics — stars: formation

1. INTRODUCTION

Cores with densities of a few 10^4 cm^{-3} and temperatures around 10 K are the basic units of low-mass star formation in nearby dark clouds like Taurus and Perseus (Myers 1995). They appear in optical images as regions of enhanced visual obscuration and in molecular line maps as relative maxima of dense gas tracers like NH_3 and CS (e.g., Myers & Benson 1983; Zhou et al. 1989). A sizeable fraction of these cores is associated with optically visible T Tauri stars or invisible *IRAS* sources ($\sim 50\%$; Beichman et al. 1986), suggesting that star formation in these systems has already taken place or is currently in progress. Cores without associated objects, referred to as "starless cores," have a less clear status. Their large number in clouds like Taurus suggests that they are stable systems and that they probably represent an early phase of core life before gravitational collapse has occurred (Beichman et al. 1986). Because core evolution may be slow, dominated by ambipolar diffusion with timescales of several Myr (Mouschovias 1977; Lizano & Shu 1989), different starless cores in a cloud will be at different stages of evolution. Some may be rather diffuse, while others may be more concentrated, about to form stars. It is even possible that some have started to collapse, but so recently that they have not have the time to form a star detectable in the far IR or the submillimeter. These more evolved starless cores (collapsing or not) will reflect primordial conditions of star formation without the perturbing effect from outflows that very quickly contaminate the spectra of even dense gas tracers (Zhou et al. 1993; Mardones et al. 1997). In this paper we present a multiline and continuum study of L1544, a core that presents many symptoms of being very advanced in its evolution toward the formation of one or more low-mass stars.

The L1544 core lies inside the Class 6 dark cloud of the same name (Lynds 1962), located in the eastern part of the

[1] Present address: Observatorio Astronómico Nacional, Campus Universitario, Apartado 1143, E-28800, Alcalá de Henares, Madrid, Spain.

Taurus molecular complex at an estimated distance of 140 pc (Elias 1978). Soon after the discovery of radio emission from interstellar molecules, L1544 was recognized as a strong source of line emission and absorption (Dieter 1973; Minn & Greenberg 1973; Cheung et al. 1973), and since then it has been a favorite target for the search for rare molecular species (e.g., Gerin et al. 1987; Bell et al. 1988; Turner & Sears 1989; Turner et al. 1990; Fuente et al. 1990). The large-scale properties of the L1544 cloud have been studied in CO by Snell (1981) and Heyer et al. (1987), and the core that it harbors has been the subject of single-pointing observations in surveys of both molecular lines (CO, Myers, Linke, & Benson 1983; NH_3, Myers & Benson 1983; HC_3N, Fuller & Myers 1993; DCO^+, Butner, Lada, & Loren 1995) and millimeter continua (Chini et al. 1984; Ward-Thompson et al. 1994). More detailed mapping observations of the L1544 core have been carried out in lines of H_2CO by Snell (1981); of NH_3 by Ungerechts, Walmsley, & Winnewisser (1982) and Benson & Myers (1983, 1989); and of HC_5N by Benson & Myers (1983) and Tolmachev (1995).

Beichman et al. (1986) did not find any *IRAS* point source associated with L1544 that fulfills their protostar selection criteria and classified this core as "starless." There is, however, a nearby *IRAS* point source, detected only at 100 μm, that has been associated with L1544: 05013+2505 (Parker 1988; Clark 1991). An inspection of the *IRAS* scans toward this source shows that the 100 μm emission lacks a pointlike component and is extended over more than 5′, coinciding with X0501+251, an object in the *IRAS* Small-Scale Structure Catalog (see also Ward-Thompson et al. 1994). The lack of a pointlike component suggests that the far-infrared emission arises from the whole L1544 core and not from an embedded self-luminous object in its interior. A similar situation occurs in many other dense cores (e.g., Wood, Myers, & Daugherty 1994). For this reason we consider L1544 as a starless core, although this of course does not rule out the presence of a very weak point source that has escaped detection by *IRAS* ($L < 0.1\ L_\odot$ for the Taurus distance; Myers et al. 1987).

2. OBSERVATIONS

We used the FCRAO 14 m telescope equipped with the QUARRY receiver array to observe L1544 in ^{12}CO (1–0), ^{13}CO (1–0), and $C^{18}O$ (1–0) during 1996 November and December; CS (2–1), $C^{34}S$ (2–1), and HCO^+ (1–0) during 1996 May and December; and N_2H^+ (1–0) during 1995 June. For the ^{12}CO (1–0) observations, we used position switching mode with a clean reference position 4°.5 away from the core, and for the rest of the observations we used frequency switching mode with offsets of 4 or 8 MHz. The back end was the FAAS autocorrelator providing velocity resolutions of 6×10^{-2} km s^{-1} (^{12}CO and N_2H^+) and 3×10^{-2} km s^{-1} (all other transitions). The T_A^* temperature scale of the telescope was converted into T_{mb} using the efficiency factors recommended by Ladd & Heyer (1996), which range from 0.41 to 0.47 for our frequencies. The beam FWHM ranges from 45″.5 at 115 GHz to 54″ at 90 GHz (Ladd & Heyer 1996).

We used the IRAM 30 m telescope to observe N_2H^+ (1–0) and H_2CO (2_{12}–1_{11}) during 1995 November and 1996 June. Both lines were observed in frequency switching mode with autocorrelators as back ends producing velocity resolutions of 3×10^{-2} km s^{-1} and 4×10^{-2} km s^{-1}. The main-beam efficiencies of the telescope were 0.73 and 0.55 for N_2H^+ (1–0) and H_2CO (2_{12}–1_{11}), and the FWHMs of the beam at these frequencies are 26″ and 17″, respectively (Wild 1995).

We used the Haystack 37 m telescope to observe C_3H_2 (2_{12}–1_{01}) in frequency switching mode during 1996 January and March. The receiver consisted of a dual-channel SIS mixer, and the backend was an autocorrelator with a velocity resolution of 5×10^{-2} km s^{-1}. The main-beam efficiency of the telescope at the C_3H_2 (2_{12}–1_{01}) frequency is approximately 0.2 (Tafalla & Myers 1997), and the FWHM of the beam is approximately 27″ (Barvainis et al. 1993).

Continuum observations at 800 μm were carried out with the single-channel UKT14 bolometer at the James Clerk Maxwell Telescope (JCMT) in service observing mode by Per Friberg during the evening of 1996 February 11. Six on-the-fly maps were done by scanning the telescope along the azimuth direction with 40″ chopping. The maps were later combined after weighting them by their expected rms noise derived from their integration time and the atmospheric attenuation (the 800 μm zenith optical depth changed from 0.4 to 0.7 during the observation). Conversion to a Jy/beam scale was done from observations of CRL 618 done before each on-the-fly map, assuming the flux density of this source is 4.2 Jy (Sandell 1994). The original data, with a resolution of approximately 13″.5, were convolved with a 20″ FWHM Gaussian to improve the signal to noise; the final resolution of our map is approximately 24″ (FWHM).

During the analysis of our line data, the need for accurate frequencies became an important issue. Differences between the values for some of our 3 mm lines in different line catalogs are as large as 40 kHz, which corresponds to about 0.13 km s^{-1}, or almost half the line width toward L1544. For this reason we have searched the literature looking for a consistent set of line frequencies. The values for the CO and CS isotopes given in Lovas & Krupenie (1974) produced the best match between the optically thin $C^{18}O$ (1–0) and $C^{34}S$ (2–1) lines, which in L1544 have similar line widths and velocity structure and must therefore be tracing almost the same gas. For this reason, we use the frequencies given by these authors: 115271.204 MHz for ^{12}CO (1–0), 110201.370 MHz for ^{13}CO (1–0), 109782.182 MHz for $C^{18}O$ (1–0), and 96412.953 MHz for $C^{34}S$ (2–1). For $C^{32}S$ (2–1), we found that the Lovas & Krupenie value is inconsistent with the observations, and we have preferred the 97980.950 MHz estimate given in the compilation of Pointer & Pickett (1985; Pointer & Pickett recommend the Lovas & Krupenie values for all the CO isotopes). For the rest of our lines, for consistency, we use the Pointer & Pickett (1985) frequencies [140839.529 MHz for H_2CO (2_{12}–1_{11}), 89188.523 MHz for HCO^+ (1–0), and 85338.893 MHz for C_3H_2 (2_{12}–1_{01})], except for N_2H^+ (1–0), for which we have preferred the more recent astronomical determination by Caselli, Myers, & Thaddeus (1995; 93176.265 MHz for the 101–012 component).

3. RESULTS

3.1. *CO Emission: The Cloud*

Both ^{12}CO (1–0) and ^{13}CO (1–0) are optically thick over most of the L1544 cloud (see below), so we rely on the thinner $C^{18}O$ (1–0) to study the large-scale distribution of gas. Figure 1 shows a series of $C^{18}O$ (1–0) velocity maps

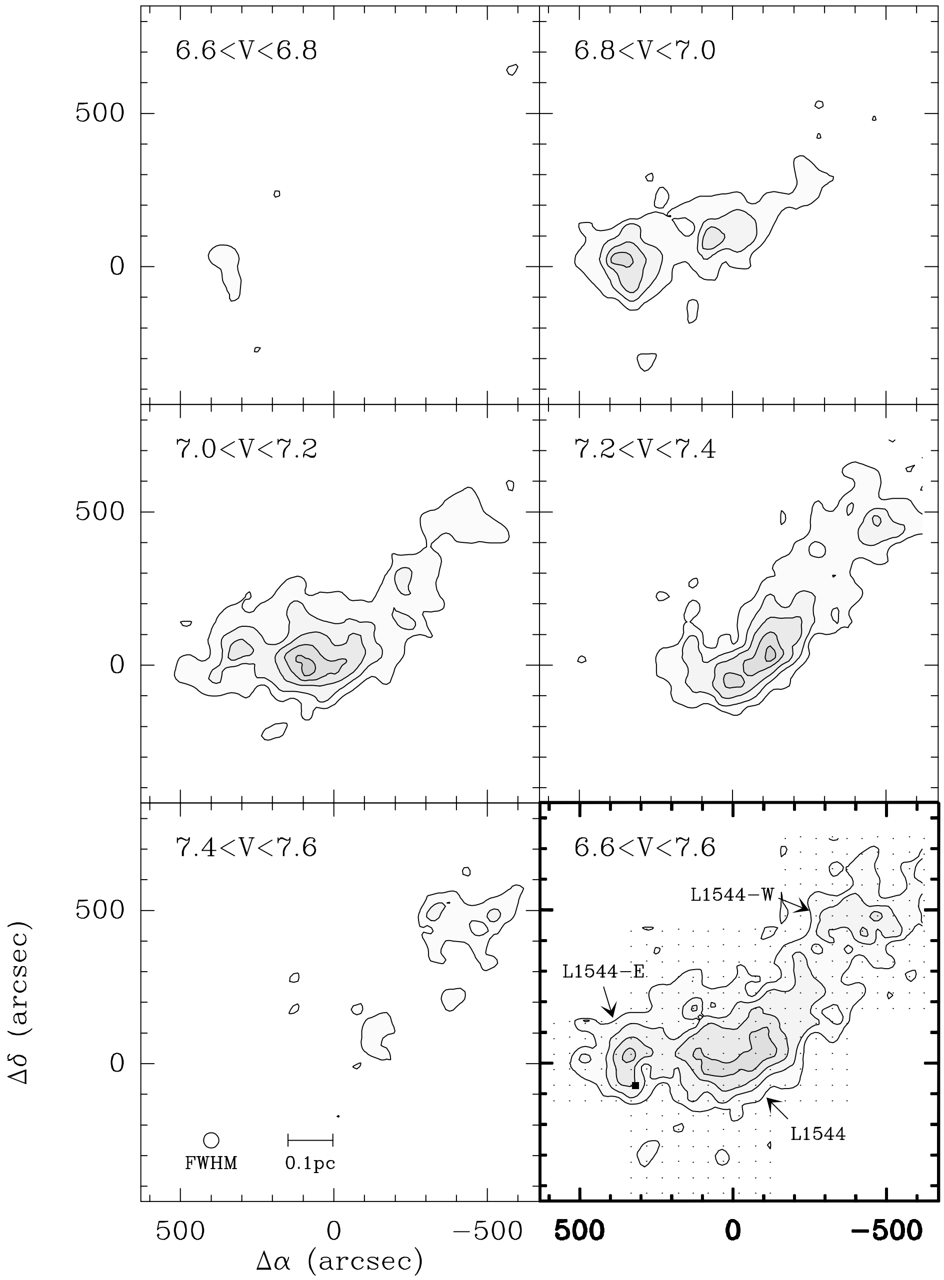

FIG. 1.—$C^{18}O$ (1–0) velocity maps every 0.2 km s^{-1} of L1544 together with an integrated map over the full velocity range in the bottom right corner. Contours are at 0.2, 0.4, ... K km s^{-1} for the velocity maps and 0.45, 0.90, ... K km s^{-1} for the full integrated map. Offsets referred to $\alpha_{1950} = 5^h1^m14^s.0$, $\delta_{1950} = 25°7'0''.0$. The filled square in the full integrated map indicates the position of the T Tauri star CIDA-8 (Briceño et al. 1993).

every 0.2 km s^{-1} together with an integrated map in the lower right-hand corner. The integrated map is in good agreement with previous maps by Snell (1981) and Heyer et al. (1987) and shows that L1544 is elongated east-west and northwest-southeast, as if it were a bent filament. It has three main condensations, approximately at (400″, 0), (0, 0), and (−400″, 500″) with respect to our central position, $\alpha_{1950} = 5^h1^m14^s.0$, $\delta_{1950} = 25°7'0''.0$. The condensation near the map center is the proper L1544 core (Ungerechts et al. 1982; Benson & Myers 1989) and will be simply referred to as L1544 in the rest of the paper. The condensations to the east and west are newly identified here and will be referred as L1544-E (east) and L1544-W (west). L1544-E seems to be associated with the T Tauri star CIDA-8 recently identified by Briceño et al. (1993) and indicated in the integrated map by a filled square, while L1544-W is not associated with any previously known stellar source.

The $C^{18}O$ (1–0) velocity maps in Figure 1 show that there is a large-scale velocity gradient across the L1544 cloud. The eastern gas has bluer velocities than the western gas, and the difference corresponds to a gradient of approximately 1.4 km s^{-1} pc^{-1}. This gradient is similar in value to the gradients found in other clouds of Taurus (Arquilla & Goldsmith 1986; Goodman et al. 1993).

We estimate the properties of the gas in the L1544 cloud from the ^{12}CO (1–0), ^{13}CO (1–0), and $C^{18}O$ (1–0) spectra that were observed with approximately the same resolution (FCRAO telescope, FWHM ≈ 46″). Our multi-isotope observations cover the central $4' \times 5'$ of the L1544 core, over which the CO emission changes only gradually, so here we present the analysis for only one point, the core center, located at ($-20''$, $-20''$); the CO spectra for that position are shown in Figure 2.

Because of the large extension of the ^{12}CO (1–0) emission (Snell 1981; Ungerechts & Thaddeus 1987), contribution from the error beam of the FCRAO antenna could be important in ^{12}CO (1–0), introducing significant uncertainty in the intensity calibration. To bracket the real ^{12}CO (1–0) brightness temperature, we use two extreme corrections, one that assumes that the source is very compact (so the brightness temperature is close to $T_{\rm mb}$, with $\eta_{\rm mb} = 0.41$, see Ladd & Heyer 1996) and the other that assumes that the source is very extended (using $T_{\rm moon}$, with $\eta_{\rm moon} = 0.70$). For the ^{13}CO (1–0) and C^{18}O (1–0) emission, because of their more limited extension (Fig. 1; see also Heyer et al. 1987), $T_{\rm mb}$ is probably the best approximation, and this is the scale used in Figure 2. Incidentally, the ^{12}CO (1–0) spectrum shown in Figure 2, as well as those from nearby positions, lacks any high-velocity wing, indicating that there is no evidence for outflow inside the L1544 dense core.

From Figure 2, the ^{13}CO (1–0)/C^{18}O (1–0) intensity ratio is 1.8, which, assuming equal excitation temperature for the two lines and a terrestrial isotopic ratio of 5.5, implies C^{18}O (1–0) and ^{13}CO (1–0) optical depths of 0.8 and 4.4, respectively. These values are in good agreement with those estimated by Myers et al. [1983; 0.6 for C^{18}O (1–0)], and as these authors used the Bell Labs telescope, which has a very clean beam pattern (Chu et al. 1978), the good agreement reinforces our assumption of a small error beam contribution to the C^{18}O and ^{13}CO FCRAO data. If the ^{12}CO/C^{18}O isotopic ratio is also terrestrial (490), the peak optical depth of ^{12}CO (1–0) is approximately 400, meaning that the center of this line traces gas from the outermost 1% of the line of sight through the molecular cloud.

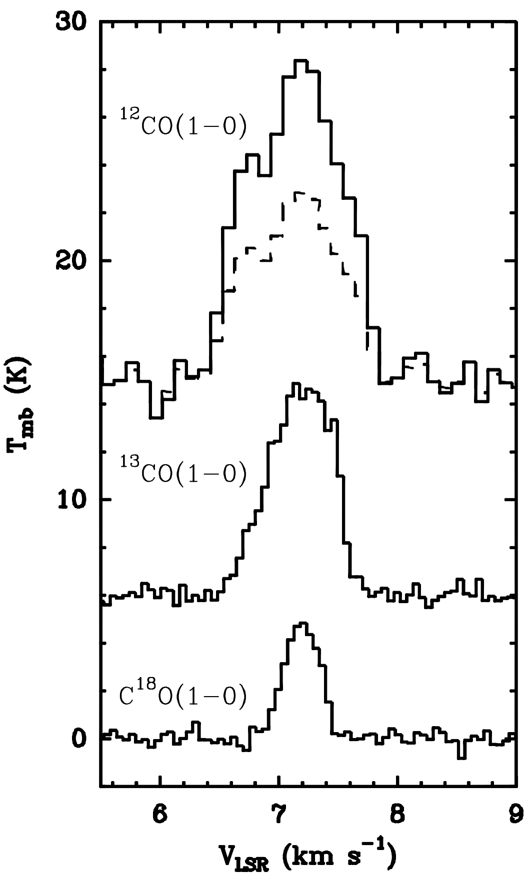

FIG. 2.—^{12}CO (1–0), ^{13}CO (1–0), and C^{18}O (1–0) toward the L1544 core center [$\alpha_{1950} = 5^{\rm h}1^{\rm m}12^{\rm s}.5$, $\delta_{1950} = 25°6'40''$, or ($-20''$, $-20''$) with respect to the origin in Fig. 1]. For ^{12}CO (1–0), both $T_{\rm mb}$ (*solid line*) and $T_{\rm moon}$ (*dashed line*) temperature scales are shown, because due to the extension of the emission, $T_{\rm mb}$ probably overestimates the real source brightness temperature (see text).

At these large optical depths, opacity broadening should be an important contribution to the line width, and to estimate its magnitude we use a simple curve-of-growth analysis (see, e.g., Phillips et al. 1979). To determine the intrinsic line width of CO, we fit a Gaussian to the C^{18}O (1–0) spectrum and correct for broadening due to $\tau = 0.8$. The result, 0.30 km s^{-1}, is then broadened, assuming optical depths of 4.4 and 400 for ^{13}CO (1–0) and ^{12}CO (1–0), predicting line widths of 0.49 and 0.90 km s^{-1} for ^{13}CO (1–0) and ^{12}CO (1–0), respectively. These values are in good agreement with the measured values of 0.62 and 0.94 km s^{-1}, showing that optical depth broadening is the main broadening mechanism for ^{12}CO (1–0) and ^{13}CO (1–0).

To determine the excitation temperature of the CO-emitting gas, we use again the ^{13}CO (1–0) and C^{18}O (1–0) spectra. The intensities in Figure 2 imply a $T_{\rm ex} = 12.5$ K, which is in good agreement with the 10 K that Myers et al. (1983) derive from CO data and Ungerechts et al. (1982) and Benson & Myers (1989) estimate from NH_3. The calibration uncertainty in ^{12}CO (1–0) propagates into an uncertainty in the excitation temperature of the outer layers of gas, which are those traced by this isotope: $T_{\rm ex} = 16.7$ K if we use $T_{\rm mb}$ and 11 K if we use $T_{\rm moon}$. As CO is most likely thermalized because of its low dipole moment, these data suggest that the gas kinetic temperature along the line of sight either remains constant or increases toward the observer. The lack of a sharp decrease in T_k will be an important element in our analysis of the dense gas in § 3.2.

Knowing the CO excitation temperature, we estimate the mass of the L1544 cloud. We use the C^{18}O (1–0) emission, assuming a C^{18}O abundance of 1.7×10^{-7} (Frerking, Langer, & Wilson 1982) and LTE excitation at 12.5 K. For the central part of L1544, where we have both ^{13}CO (1–0) and C^{18}O (1–0) spectra, we use the optically thin approximation corrected by a factor $\tau/(1 - e^{-\tau})$ derived from the ^{13}CO/C^{18}O intensity ratio. For the rest of the cloud, which probably has $\tau \ll 1$ (Heyer et al. 1987), we use the optically thin limit without further correction. Assuming 10% He abundance and a distance of 140 pc, we estimate a total cloud mass of 28 $M_\odot$, in excellent agreement with Snell's (1981) estimate corrected for our assumed distance (25 $M_\odot$). In order to measure the masses of the individual cores, we use as boundaries of L1544 and L1544-E the 1.35 K km s^{-1} contour in the integrated C^{18}O (1–0) map of Figure 1 (the lowest contour for which the cores appear as separate entities). For L1544-W, which is more diffuse and therefore less defined, we use the 0.9 K km s^{-1} contour (see Fig. 1). Applying τ correction factors to the optically thin limit for L1544 and L1544-E (but not for L1544-W), we estimate masses of 8, 1.5, and 1.3 $M_\odot$ for L1544, L1544-E, and L1544-W, respectively. Slightly more than one-third of the total cloud mass, therefore, resides in the main L1544 condensations, and about 0.7 of the mass of the three main condensations is in L1544.

3.2. *Dense Gas Emission: The Core*

We study the distribution of the dense gas in L1544 using molecular species with high dipole moment ($\mu \geq 2$ D). Figure 3 presents the spectra toward the core peak for six such molecules: HCO^+ (1–0), H_2CO (2_{12}–1_{11}), CS (2–1), C_3H_2 (2_{12}–1_{01}), N_2H^+ (101–012), and $C^{34}S$ (2–1). These spectra form an approximate sequence of optical depth increasing upward and present shapes very different from those of CO in Figure 2. The thinnest line, $C^{34}S$ (2–1), is approximately Gaussian (not exactly; see below) centered at $V_{LSR} = 7.2$ km s^{-1}, while the other lines show two peaks with a dip at the velocity of the $C^{34}S$ (2–1) peak or, in the case of HCO^+ (1–0), a single peak blueshifted from the $C^{34}S$ (2–1) peak. This coincidence of the thin line peak with the thick line dip indicates that the two maxima in the thick spectra arise from self absorption and not from two different clouds lying along the line of sight. In the case of HCO^+ (1–0), the self absorption is so broad (probably because of saturation) that the red component is totally missing, and all that is left in the spectrum is a weak component toward the blue.

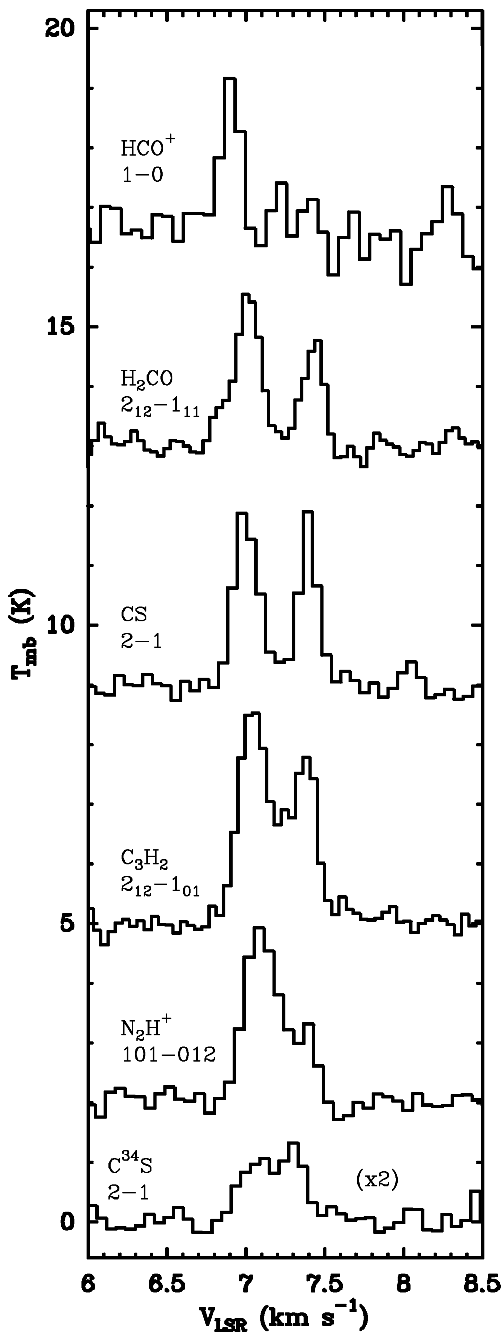

FIG. 3.—Spectra of dense gas tracers toward the core center (same position as in Fig. 2) ordered approximately by optical depth increasing upward. The two peaks in the thick spectra result from self absorption, because the dip between them coincides with the peak of the thinner $C^{34}S$ (2–1) at the bottom of the figure. In the extremely thick HCO^+ (1–0), the self absorption is so broad that the red component is completely missing.

In order for the intensity at the center of the HCO^+ (1–0), H_2CO (2_{12}–1_{11}), CS (2–1) lines to be almost zero, the absorbing gas has to be very optically thick and have an excitation temperature close to that of the cosmic background. As the gas kinetic temperature along the line of sight is constant or increases outward (§ 3.1), the low excitation temperature of the dense gas tracers must arise from subthermal excitation. This means that the gas in the core has a strong density gradient, with a high-density inner part and a low-density outer region. In § 3.3.2 we will exploit this effect to estimate the slope of the gradient.

3.2.1. *Distribution of the Emitting Gas*

Because of the self absorption in the common molecular species, we have to rely on the less abundant molecules to study the dense, emitting gas. $C^{34}S$ (2–1) is probably optically thin (see Fig. 3). N_2H^+ (101–012) presents complicated, non-Gaussian spectra toward the core center that suggest self absorption or more than one component. Away from the center, however, the lines are symmetric and a hyperfine fit to the core average spectrum gives a mean (101–012) optical depth of 0.5 (the value toward the center is approximately 1), so N_2H^+ (1–0) is at most marginally thick on L1544. The dust continuum emission at 800 μm is also optically thin, as for $\kappa_{800\,\mu m} = 0.01$ cm^{-2} g^{-1} (Preibisch et al. 1993); we would need $N(H_2) > 10^{25}$ cm^{-2} to reach unity optical depth, which is orders of magnitude larger than our estimate from $C^{18}O$ (1–0) (§ 3.1). We therefore base our analysis on these three tracers.

Figure 4 presents maps of $C^{34}S$ (2–1) (FCRAO), N_2H^+ (1–0) (FCRAO and IRAM 30 m data), and 800 μm continuum (JCMT) toward L1544. All show a well-defined emission peak that in the best sampled (N_2H^+) maps lies near ($-20''$, $-20''$) and is slightly elongated northwest-southeast. This sense of elongation is also seen in the NH_3 (1, 1) map of Ungerechts et al. (1982) and the HC_5N (9–8) map of Tolmachev (1995), and it approximately matches the large-scale elongation of the $C^{18}O$ (1–0) map (Fig. 1). The $C^{34}S$ (2–1) emission is more extended than N_2H^+ (1–0), an effect that recalls the larger extension of CS versus NH_3 noticed by Zhou et al. (1989; see also Pastor et al. 1991; Myers et al. 1991). It most likely results from a difference in abundance between the two species.

The 800 μm map does not show evidence for an unresolved pointlike component, in good agreement with our assumption that L1544 is starless. (Our peak flux of 470 mJy per 13''.5 beam agrees very well with the flux measured by Ward-Thompson et al. 1994 with a single pointing.) In contrast with other starless cores, however, a radial average of the emission around the peak ($-20''$, $-20''$) follows a single power law of index -0.7 ± 0.2 (correlation coeffi-

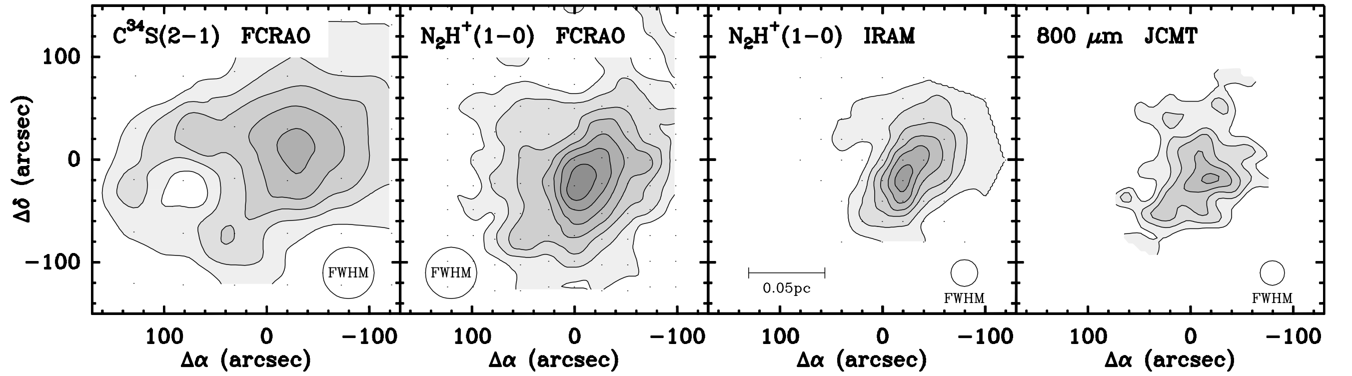

FIG. 4.—*Left panel:* Map of $C^{34}S$ (2–1) emission integrated between 6.6 and 7.6 km s^{-1}. Contours are at 0.05, 0.1, ... K km s^{-1}. *Center panels:* Map of the N_2H^+ (1–0) emission observed with FCRAO integrated over all seven hyperfine components (to enhance signal to noise). Contours are at 0.5, 1, ... K km s^{-1}. *Right panel:* Map of the emission from the 101–012 (isolated) component of N_2H^+ integrated between 6.6 and 7.6 km s^{-1} (IRAM 30 m data). Contours are at 0.15, 0.30, ... K km s^{-1}. Offsets referred to same origin as in Fig. 1.

cient 0.9), which is different from the two power laws that Ward-Thompson et al. (1994) and André, Ward-Thompson, & Motte (1996) need to fit the profiles of other starless cores in Taurus and Ophiuchus (a shallow-distribution one toward the center and a steep one toward the outside). The continuum distribution of L1544 is more similar to that found in cores with stars, for which Ladd et al. (1991) fitted single power-law profiles with index ≈ -1.0. This suggests that L1544 is slightly more concentrated than starless cores, but slightly less concentrated than cores with stars. If this is the case, it could represent evidence for L1544 being at a more advanced stage of evolution than other starless cores. Theories of core formation suggest that cores evolve from an initial extended configuration to a state of high central concentration via ambipolar diffusion, and that the time-scale for this process is 10^6–10^7 yr (Mouschovias 1977; Lizano & Shu 1989). It is therefore possible that L1544 is near the end of this ambipolar diffusion phase and is close to the point of forming one or more stars.

3.2.2. *Mass and Kinematics of the Emitting Gas*

We estimate the mass of dense gas in L1544 both from the molecular and continuum emissions. Using the radius of the N_2H^+ (1–0) map (0.025 pc) and the mean line width (0.37 km s^{-1}), we estimate a virial mass of 0.7 $M_\odot$, similar to the 0.6 $M_\odot$ estimated by Ungerechts et al. (1982) and the 1.2 $M_\odot$ estimated by Benson & Myers (1989), both from NH_3. This mass, however, is only a lower limit, since the core does not end at the half-power radius and contains a lower density envelope of about 8 $M_\odot$ (§ 3.1). From the 800 μm integrated flux and assuming a $\kappa_{800\,\mu m} = 0.01$ cm^{-2} g^{-1} (Preibisch et al. 1993), we derive a core mass between 2 and 6 $M_\odot$, depending on whether the dust temperature is 12 or 8 K. Although larger than the virial mass, this value is consistent with it, because uncertainties in dust properties propagate into errors of up to a factor of 5 in mass estimates (Preibisch et al. 1993)

To study the kinematics of the dense gas, we use $C^{34}S$ (2–1), probably our thinnest line tracer, and present in Figure 5 velocity maps every 0.2 km s^{-1} for the same velocity intervals we used for $C^{18}O$ (1–0). As the maps show, the $C^{34}S$ (2–1) emission changes from being approximately east-west in the $7.0 < V < 7.2$ range to being northwest-to-southeast in the $7.2 < V < 7.4$ map. This change in orientation matches that seen in the $C^{18}O$ (1–0) maps (Fig. 1), and it can also be seen in equivalent N_2H^+ (1–0) maps but with a weaker eastern emission. To investigate its origin, we have inspected the individual $C^{34}S$ (2–1) spectra, and present them in Figure 6 as a function of position. As the figure shows, spectra from the north, east, and south are narrow (FWHM approximately 0.2 km s^{-1}), while spectra from the center and west are almost twice as broad. The narrow lines seem to come with two possible velocities: V_{LSR} of 7.10 (northeast) and 7.25 km s^{-1} (south), while the broad spectra have intermediate velocities. If gas rotation were the explanation for the observed line changes, we would expect to find the intermediate velocities between the extreme ones, but this seems not to be the case. Neighboring positions like (80, −20) and (30, −70) have LSR velocities of 7.10 and 7.24 km s^{-1}, while the broad intermediate spectra are located toward the western edge. This suggests a more complicated velocity pattern. One possibility is that there are two different velocity components in the gas, one at 7.10 and the other at 7.25 km s^{-1}, which overlap toward the center and west, producing broad, non-Gaussian spectra at intermediate velocities. To test this interpretation, we have fitted two Gaussians to each $C^{34}S$ (2–1) spectrum, finding that the broad spectra in fact seem composed of the same two components identified as isolated in the narrow spectra (fit results are shown by thin curves in Fig. 6). The distribution of these components is approximately like that shown in the two central maps of Figure 5, because the velocity intervals approximately coincide with the velocities of the components.

The presence of two components does not contradict the fact that the CS (2–1) lines suffer from self absorption. Self absorption is unavoidable in explaining the CS (2–1) (and other thick) spectra because of the prominence of the two peaks, their separation in velocity, and the fact that the $C^{34}S$ (2–1) spectrum, even with its two components, lies filling dip of the CS (2–1) line. The two $C^{34}S$ components are too close in velocity to produce a double-peaked spectra, and it is only because there are positions where we see them isolated that we can be sure they represent physical entities. The data from L1544, therefore, imply that the background emitting gas has two velocity components that overlap at some positions, but do not exactly coincide. In front of them (between them and us), there is another component of very subthermally excited gas at much lower density. This component absorbs the rather kinematically

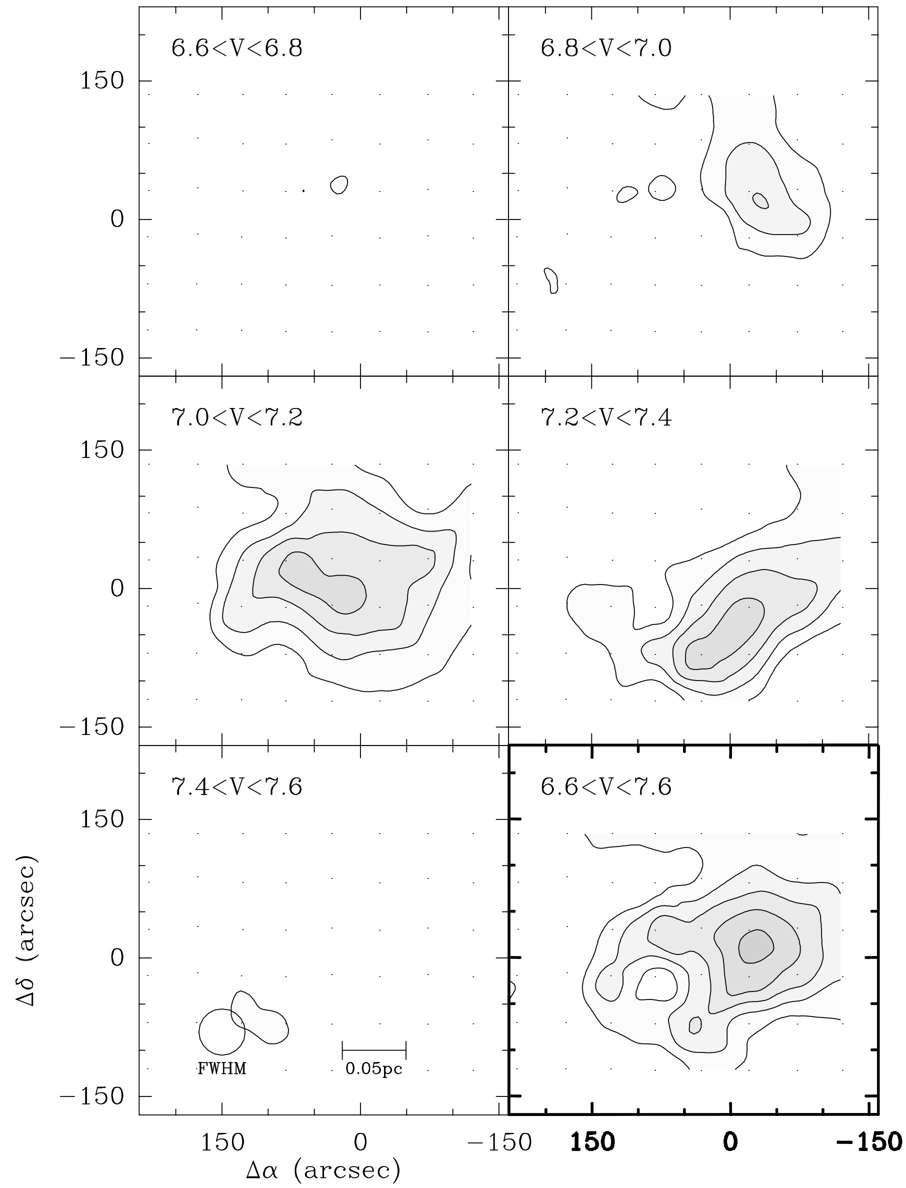

FIG. 5.—$C^{34}S$ (2–1) velocity maps every 0.2 km s^{-1} together with a full integrated intensity map in the bottom right corner. Contours are at 0.025, 0.05, … K km s^{-1} for the velocity maps and 0.05, 0.1, … K km s^{-1} for the full integrated maps. Offsets referred to the same origin as in Fig. 1.

complicated emission from the background gas and gives rise to the very deep dips in the spectra of optically thick lines. In § 3.3 we will show that this picture we propose not only explains the qualitative appearance of the lines toward the center, but can be used to predict with reasonable accuracy the intensity and line shape for all CS (2–1) spectra based in the $C^{34}S$ (2–1) lines.

3.2.3. *The Absorbing Gas*

The foreground absorbing gas cannot be mapped like the background gas, because its low excitation makes it almost invisible. Its presence is only revealed by its absorbing effect on the background emission, so it has to be studied directly from the self-absorbed spectra. Figure 7 presents maps of spectra for CS (2–1), H_2CO (2_{12}–1_{11}), and C_3H_2 (2_{12}–1_{01}), three of our four optically thick dense gas tracers. [HCO^+ (1–0), because of its extreme self absorption, only shows a blue peak where detected.] The larger scale CS (2–1) map shows that the self absorption extends over more than 300″ (>0.2 pc) and affects all the CS emission from the L1544 core. There is also CS emission associated with L1544-E (not shown in Fig. 6), but it is single-peaked, has the same velocity as $C^{34}S$ (2–1) and $C^{18}O$ (1–0), and so is not self-absorbed.

In principle, the absorbing material could lie superposed by chance on the L1544 core, although the fact that its velocity is almost equal to that of the core suggests that this is unlikely. To study further the relation between emitting and absorbing gases, we use the C_3H_2 spectra, which are only moderately self-absorbed and therefore sensitive to changes in the column density of absorbing gas (Fig. 3). Figure 7 (*bottom panel*) shows that the C_3H_2 line at the core center is double-peaked, while positions 60″–80″ away in all four directions have single-peaked spectra. At all these off-centered positions, the C_3H_2 single line peaks between the two peaks of the self-absorbed CS and H_2CO, as if the C_3H_2 lines were optically thin. Furthermore, toward the west and north, the only two directions with detectable $C^{34}S$ (2–1) and N_2H^+ (1–0), the C_3H_2 lines have the same

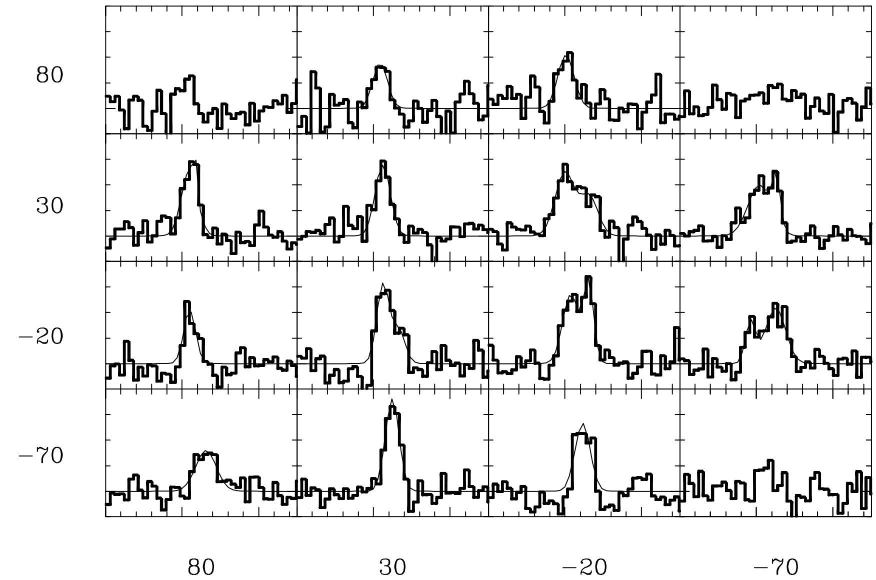

FIG. 6.—$C^{34}S$ (2–1) spectra toward the center of L1544 as a function of position (*histogram*) with two component Gaussian fits superposed (*connected lines*). In each spectrum the intensity scale goes from −0.1 to 0.8 K (T_{mb}) and the velocity scale from 6 to 8.5 km s^{-1}. The numbers around the external box indicate the positions of the spectra in arcsecond offsets with respect to our central position (see Fig. 1). The grid was centered in (−20″, −20″), the N_2H^+ (1–0) maximum (see Fig. 4).

velocity as the thin $C^{34}S$ and N_2H^+. This shows that the C_3H_2 line changes from being thick and self-absorbed at the core center to being thin and single-peaked away from it, and this means that the column density of absorbing gas decreases with distance from the core peak. Thus, both the absorbing and the emitting gas are centrally concentrated, and this suggests that there is a physical relation between the two. The most likely situation is that each component represents a different region of a centrally concentrated core, with the emitting gas representing the denser, inner part and the absorbing material being the outer, lower density layers.

The relative velocity between the emitting and absorbing layers is reflected in the intensity contrast between the peaks of the self-absorbed profiles. A line profile with brighter blue peak indicates that the foreground absorbing gas is slightly redshifted with respect to the background emitting gas, so the two components are approaching each other. The opposite case occurs for a line profile with brighter red peak (for detailed modeling, see Leung & Brown 1977; Leung 1978; Bernes 1979; Walker et al. 1986; Walker, Narayanan, & Boss 1994; Myers et al. 1996). As Figure 7 shows, the CS spectra in L1544 have predominantly brighter blue peaks over most of the core; from 21 asymmetric CS (2–1) spectra, 18 have brighter blue peak and only 3 have brighter red peak. The H_2CO data show a similar spatial distribution of the line asymmetry, and of the 39 asymmetric spectra with sufficient signal-to-noise ratio, 36 are blue and three are red. This prevalence of brighter blue–peak spectra indicates that the absorbing and emitting components are moving toward each other, and that inward (approaching) motions prevail over most of the dense core.

The gas kinematics in L1544, however, is not as simple as if the core consisted of just two layers of constant velocity gas approaching each other. The relative intensity between the CS (2–1) peaks changes over the core, so changes in the front-back relative velocity have to be rather common. We have seen in § 3.2.2 that the background emitting gas consists of two velocity components with slightly different spatial distribution. It is tempting to explain the sudden changes in the CS (2–1) spectra as the result of the kinematics of the background gas. In the next section we present a simple model that proves this is the case.

3.3. *Analysis and Modeling of the Spectral Lines*

The two main spectral peculiarities of L1544 are the presence of deep self absorptions in the thick lines of the dense gas tracers, but not in CO, and the strong variation with position of the peak contrast in the self-absorbed profiles (with a majority of brighter blue peaks). In this section we investigate these two peculiarities using simple radiative transfer modeling. Our goals here are (1) to determine whether a simple density gradient can reproduce the observed selective self absorption and (2) to understand the origin of the spatial variations of the line profiles in terms of motions of the foreground and background gas.

Even such a modest project requires some simplification, as the simultaneous modeling of the spectra at all cloud positions would need a three-dimensional radiative transfer code with a prohibitively large number of free parameters. Fortunately, we can divide the line-modeling problem into two separate, almost orthogonal parts: the study of the kinematical line variations across the map (i.e., perpendicular to the line of sight) and the characterization of the physical conditions along a given line of sight. These two problems can be solved separately, because under typical cloud conditions, the molecular excitation depends very weakly on the exact line-broadening mechanism (White 1977), while the detailed appearance of a self-absorbed line profile depends more on the gas kinematics than on the details of the excitation (Myers et al. 1996). This means that for estimating the gas density gradient we can use a model with simple kinematics, while for studying the spatial variations of the gas velocity what we simplify is the radiative transfer. We start studying the gas kinematics, because the modeling is simpler.

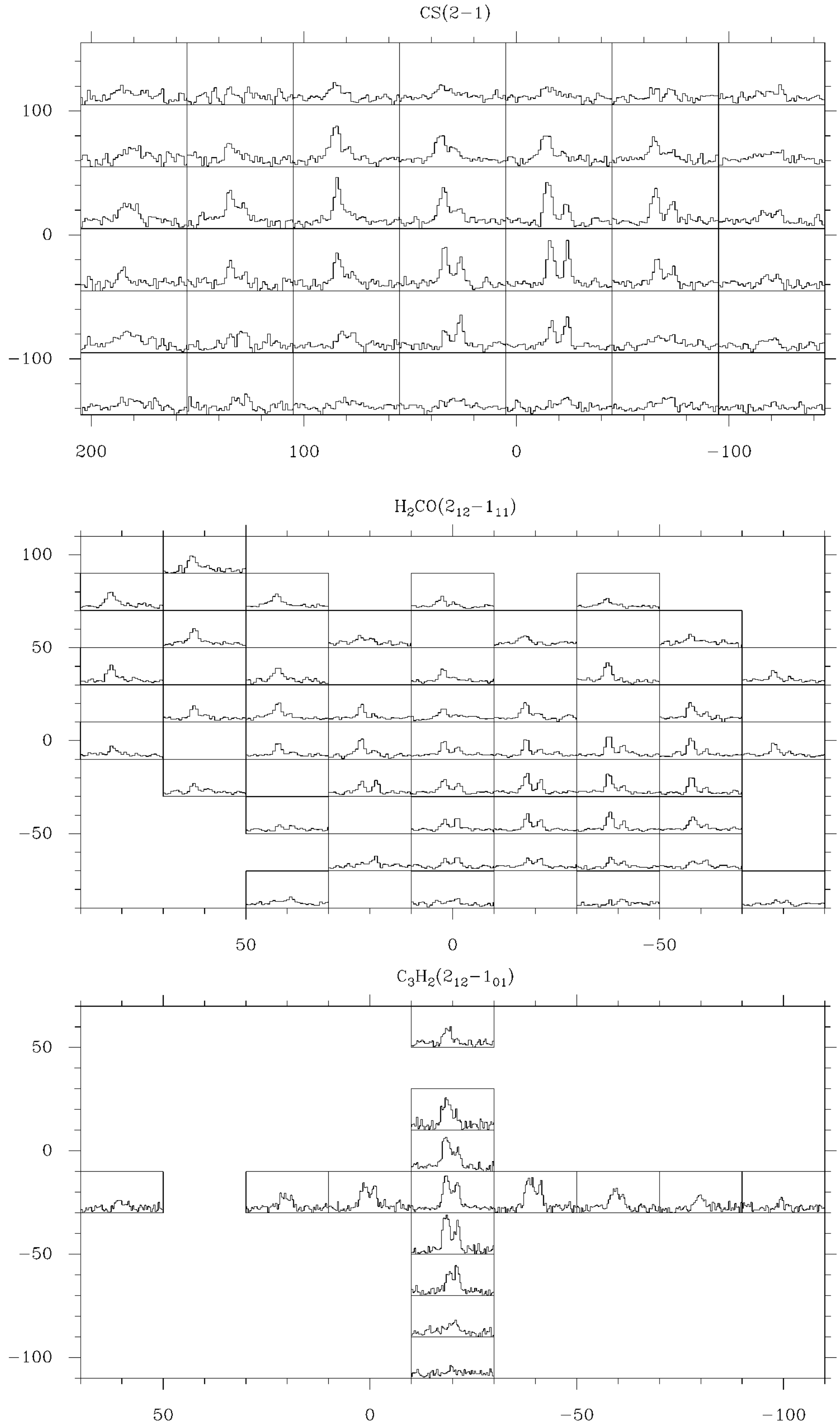

FIG. 7.—Maps of spectra for CS (2–1) (*top*), H_2CO (2_{12}–1_{11}) (*middle*), and C_3H_2 (2_{12}–1_{01}) (*bottom*). In all cases, the velocity ranges from 6 to 8.5 km s^{-1} (LSR) and the intensity from −0.5 to 4 K (T_{mb}). Note that the CS (2–1) map extends over a larger area than the H_2CO (2_{12}–1_{11}) and C_3H_2 (2_{12}–1_{01}) maps, which are more restricted and have higher angular resolution. The CS (2–1) spectra show evidence for self absorption over more than 300″, while the C_3H_2 (2_{12}–1_{01}) spectra make a transition from self-absorbed toward the core center to optically thin at large radii. Offsets referred to the same coordinates as in Fig. 1.

3.3.1. *Kinematics*

Our goal here is to study the changes in the relative velocity between the absorbing and emitting components, and for that we concentrate on the CS (2–1) lines, which show deep self absorptions and systematic changes in the peak contrast (Fig. 7). We model the L1544 cloud with two layers, a background one that emits and a foreground one that absorbs, and leave the details of the excitation for the discussion in the next section. This type of two layer model is similar to those presented by Myers et al. (1996) and Ramesh, Bronfman, & Deguchi (1997), but here we adopt a more empirical approach and use the observed $C^{34}S$ (2–1) spectra to model the CS (2–1) emission from the background gas. The $C^{34}S$ (2–1) spectra are most likely optically thin (§ 3.2.1), so they must represent (except for a scaling factor) the CS (2–1) lines the cloud would emit if were not for the absorption by foreground gas. Thus, we assume that at each map position the background gas emits a CS (2–1) spectrum equal to the observed $C^{34}S$ (2–1) spectrum except for a scaling factor X that we take as constant over the core and is a free parameter. Because of the low signal-to-noise ratio of the $C^{34}S$ (2–1) spectra, we do not use the real channel values to simulate the emission, but the Gaussian fits to the line profiles presented in § 3.2.2 (Fig. 6). The relative intensity and velocity of the two components in the $C^{34}S$ (2–1) spectra are in this way input automatically to the model without using any adjustable parameter.

We model the foreground gas assuming it is a purely absorbing screen that has constant velocity, width, and optical depth over the cloud. Its effect on the background emission is therefore to attenuate it by the factor

$$\exp\{-\tau_0 \exp[-4\ln 2(v - v_0)^2/\Delta V^2]\},$$

where τ_0, v_0, and ΔV are the three additional free parameters of our kinematic model.

For each position with detected $C^{34}S$ (2–1) (13 in total), we use our four-parameter model to predict the emerging CS (2–1) spectrum, and in Figure 8 we present the result for the following choice of parameters: $v_0 = 7.20$ km s^{-1}, $\Delta V = 0.22$ km s^{-1}, $\tau_0 = 2.7$, and $X = 10$. As the figure shows, the model correctly predicts the observed changes in the CS (2–1) line profiles across the core. In particular, it reproduces the sense of peak asymmetry at most positions, including the reversal toward (30″, −70″) and the single peaks near (80″, 30″). At those extreme positions, the velocity difference between background and foreground gas is larger than half the line width, and the red side of the line is fully suppressed by the absorption. The success of our model confirms that the CS (2–1) spectra are strongly self-absorbed by foreground gas. It also shows that the changes in the peak contrast result from motions in the background material and not in the absorbing gas. Because this background material in the two-layer model represents the gas in the core interior, the line changes arise from inner core kinematics and not from velocity changes in the core outer layers.

We can use the velocity derived for the foreground gas and the centroid velocity of the background gas to estimate a relative front-back velocity for each map position. Although the inward motion interpretation rests on the asymmetry of the self-absorbed spectra and is therefore independent on the exact frequency of the lines, the estimate of the front-back velocity difference using the two-layer model is limited by the uncertainty in the relative frequency of CS (2–1) and $C^{34}S$ (2–1) (see § 2). It is difficult to estimate this uncertainty, but from the lack of systematic wing emission in our model (Fig. 8) and a comparison of the wing velocities of CS (2–1) and $C^{34}S$ (2–1), we estimate that it corresponds to a velocity uncertainty smaller than the channel width (0.03 km s^{-1}). The uncertainty in the size of the velocity changes across the core is of course much smaller, at least by a factor of a few. Thus, using our model, we derive a relative approaching speed of 0.10 km s^{-1} toward the northeast (where the peak contrast is largest) and 0.01 km s^{-1} toward the center (where the contrast is small). This latter value, at the limit of the model precision,

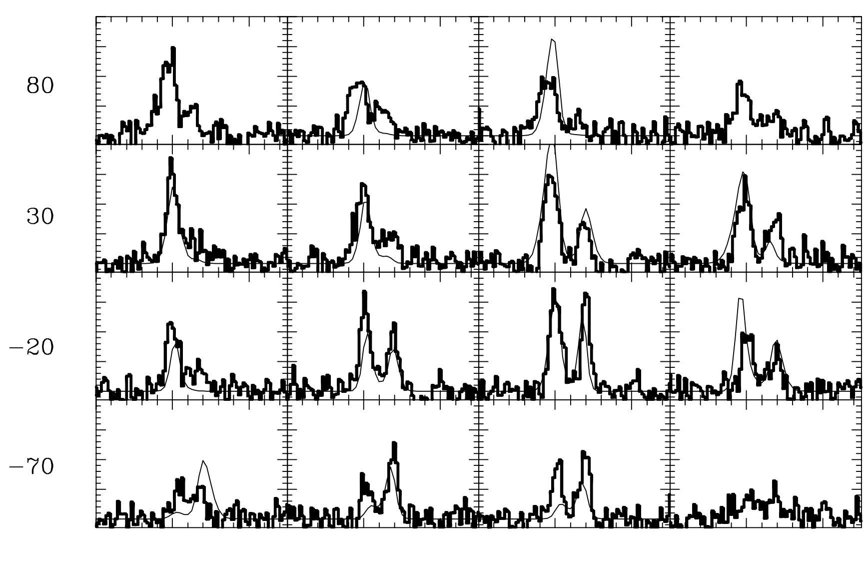

FIG. 8.—CS (2–1) spectra toward the center of L1544 as a function of position (*histogram*) compared to the predictions of our two-layer model (*connected line*) using the $C^{34}S$ (2–1) fits from Fig. 6. The intensity scale goes from −0.3 to 4 K (T_{mb}) and the velocity scale from 6 to 8.5 km s^{-1}. Offsets and grid as in Fig. 6. Positions with no model prediction do not have enough signal to noise in $C^{34}S$ (2–1) to allow a Gaussian fit (see Fig. 6).

is in good agreement with the 0.006 km s^{-1} that Myers et al. (1996) estimate toward the same position using their simple analytic model. The outward motions to the south are of about 0.03 km s^{-1} and affect only a small fraction of the L1544 core gas.

Although our model is purely kinematic, the best values of the free parameters are physically meaningful. The X factor represents the ratio between CS (2–1) and $C^{34}S$ (2–1) intensities from the background layer, and our $X = 10$ value is consistent with having a terrestrial abundance ratio (22.5) and a slightly optically thick CS (2–1) emission in the background gas ($\tau \approx 2$) or having an optically thin background emission and an abundance ratio of 10, like the value found by Mundy et al. (1986) in several star-forming regions. The value of $\tau_0 \approx 3$ for CS (2–1) in the absorbing gas, on the other hand, implies that our assumption that this gas is optically thin in $C^{34}S$ (2–1) is self-consistent. Finally, the line width of the absorbing component is very close to the line widths measured for the individual $C^{34}S$-emitting components in § 3.2.2. This again shows that very likely all components are physically related.

3.3.2. *Cloud Structure*

Having studied the spatial variations of the gas kinematics across the core, we now turn our attention to the conditions necessary to produce deep self absorptions in CS and none in CO. These spectral signatures appear everywhere in the L1544 core, so they cannot depend on the details of the gas velocity field studied in the previous section. For this reason, we now simplify the kinematics of the model and concentrate on the molecular excitation. We assume the cloud is spherical and its velocity field consists of a turbulent component (described below) and a constant inward velocity of 0.01 km s^{-1}, as deduced in the previous section for the central core position. Our goal here is to simultaneously reproduce the ^{12}CO, ^{13}CO, $C^{18}O$, CS, and $C^{34}S$ spectra observed with the FCRAO telescope, because they constitute a homogeneous set coming from the same telescope and having similar calibration. Because of the very different dipole moments of CS and CO, these data are sensitive to both the high- and low-density gas. In addition, the combination of abundant and rare isotopic species for each molecule makes the data sensitive to a large range of optical, and therefore physical, depths along the line of sight.

To better constrain the core conditions, we model the spectra both toward the cloud center ($R = 0''$) and toward $R = 50''$ (one FCRAO beam width), which we take as the average of the spectra 50″ away from the center in all four directions. We solve the equations of statistical equilibrium and radiative transfer using the Monte Carlo code written by Bernes (1979), to which we have incorporated collisional coefficients for CO from Flower & Launay (1985) and for CS from Turner et al. (1992), and a convolution routine to simulate observational beam smoothing. We set the outer radius at 5×10^{17} cm, corresponding to 240″ at the distance of 140 pc (see Fig. 1), and from the CO analysis in § 3.1 we assume the gas kinetic temperature increases linearly from 11 K at the center to 13.5 K at the outer edge. As a compromise between the two possible calibrations of the ^{12}CO (1–0) spectrum (§ 3.1), we use an efficiency factor of 0.53, the geometrical mean of $\eta_{\rm mb}$ and $\eta_{\rm moon}$. Finally, we model the presence of two overlapping velocity components in the core interior and one in the outer layers by using a single broad line (thermal width plus a turbulent component with FWHM of 0.25 km s^{-1}) in the inner one-third of the core and a narrower component (thermal width plus a 0.125 km s^{-1} turbulent component) in the rest.

In order to fit the data, we have explored power-law density profiles ($n \sim r^{\alpha}$) with α equal to -2, -1.5, and -1. For each value of α, several combinations of the line width, molecular abundance, and other core parameters were tried. The optically thin transitions [$C^{34}S$ (2–1) and $C^{18}O$ (1–0)], which decrease slowly in intensity from the center to $R = 50''$, rule out $\alpha = -2$ or steeper density profiles, except if the molecular abundance is allowed to decrease inward to compensate for the sharp density increase. On the other hand, $\alpha = -1$ or flatter density profiles do not reproduce the self-absorbed CS (2–1) lines, because they cannot combine the large column density of low excitation CS in the outer layers, necessary to produce the deep dip in the line, and at the same time have the rather high central density needed to reproduce the bright CS peaks. Again, this problem can be eased by allowing a variable CS abundance (this time increasing inward).

If we discard strong abundance variations with radius, our modeling favors $\alpha = -1.5$ density profiles, which allow reasonable fits using constant molecular abundances and terrestrial isotopic ratios [$X(\mathrm{CS})/X(\mathrm{C^{34}S}) = 22.5$, $X(^{12}\mathrm{CO})/X(^{13}\mathrm{CO}) = 89$, $X(^{13}\mathrm{CO})/X(\mathrm{C^{18}O}) = 5.5$]. In Figure 9 we show the results for a model that fits reasonably well the observations and has the following parameters: $X(\mathrm{C^{18}O}) = 1.7 \times 10^{-7}$ (as in Frerking et al. 1982), $X(\mathrm{CS}) = 9 \times 10^{-9}$, and $n(r = 5 \times 10^{17}$ cm$) = 2 \times 10^3$ cm^{-3}. Despite the rather good fit, the model deviates from the data in two systematic ways. First, the $C^{34}S$ (2–1) model emission drops slightly too fast with radius, suggesting that the density profile flattens somewhat near the core center. Second, the observed CO spectra are broader and less Gaussian than the model predicts. This may in part result from our simplified treatment of the inner core kinematics with a single broader Gaussian instead of with two Gaussians side by side, because it would correspond to multiple components and produce a more rectangular profile. Still, it is remarkable that such a variety of line profiles and intensities can be fitted simultaneously with a simple model like ours.

The parameter determination presented here is not unique, and a few other combinations of outer radius, outer density, and molecular abundance can also fit the data. Some results of the modeling, however, are independent of the exact choice of these parameters, and we summarize them as follows: First, the fits of Figure 9 illustrate that it is possible to model both the CO and CS spectra with a single set of physical conditions, and that the CS self absorption is caused by core gas and not by an unrelated component that lies along the line of sight. Second, the width differences between the spectra of the CO isotopes (especially toward the center) naturally arise from their different optical depths, even for a static cloud model where the turbulent line width increases inward. Third, the self absorption in CS (2–1) arises from gas in the outer cloud layers that has a density of several times 10^3 cm^{-3} and is strongly subthermally excited. The low energy levels of the CO isotopes are still thermalized in this gas, in part thanks to photon-trapping for the abundant ^{12}CO and ^{13}CO. As the excitation temperature of the CO lines is expected to decrease with rotational J number, our model predicts that high J

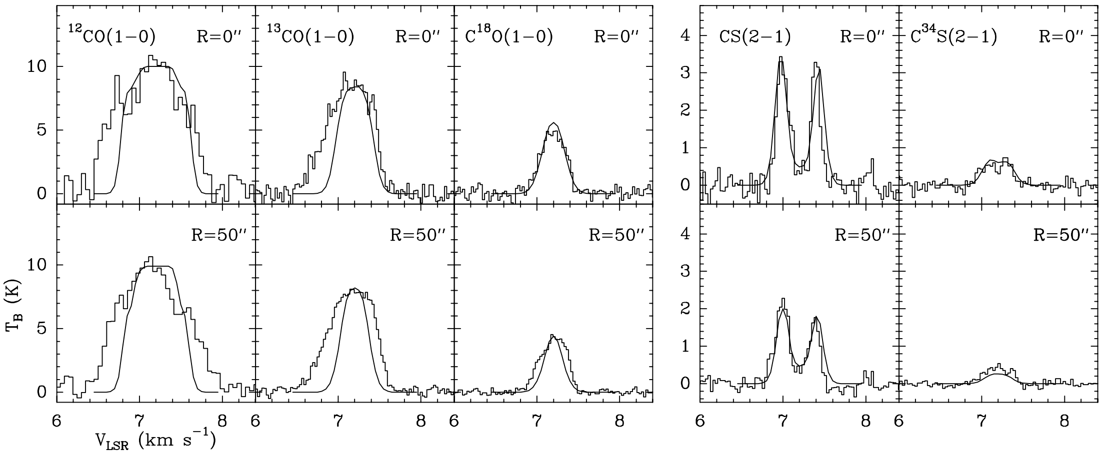

FIG. 9.—Comparison of observed FCRAO spectra toward L1544 for $R = 0$ and $R = 50''$ (*histogram*) and the results of the radiative transfer model described in the text (*connected line*).

^{13}CO transitions will present self absorption at the line center (the 2–1 transition is not self-absorbed but extremely flat-topped, following the expected trend, according to our own IRAM 30 m unpublished observations). Finally, our model favors density power laws with an index near $\alpha = -1.5$. It is interesting to note that this is the power law predicted by models of collapsing clouds, both for an initial singular isothermal sphere ($n \sim r^{-2}$; Shu 1977) and for a logotropic sphere ($n \sim r^{-1}$; McLaughlin & Pudritz 1996, 1997).

4. DISCUSSION

4.1. *L1544 in Relation with Other Cores*

L1544 is not the only starless core whose dense gas tracer lines present self-absorbed spectra with brighter blue peak. The recent survey of 24 starless cores in the lines of CS and N_2H^+ by Lee et al. (1998) shows that this spectral feature occurs in a moderate fraction of systems (4/24, including L1544) and never with the extreme depth with which it is observed in L1544. Probably the starless core most similar to L1544 is L1498, also in the Taurus complex. Lemme et al. (1995) found double-peaked spectra with brighter blue peaks in CS (3–2); although from their data they cannot distinguish between having two components or suffering from self absorption. The recent observations of Lee et al. (1998) suggest that self absorption is in fact the cause of the double peak in L1498, which together with the $n \sim r^{-1.5}$ density law that Lemme et al. (1995) estimate from their $C^{18}O$ data, makes the two cores seem rather similar and good candidates for gravitational infall. In fact, the detailed study by Kuiper et al. (1996) suggests that the outer envelope of L1498 is still growing and that the core is close to gravitational instability. The deeper CS self-absorption of L1544 suggests that L1544 is more advanced in its evolution to become a star-forming core.

Several cores with stars have strongly self-absorbed spectra with brighter blue peaks in dense gas tracer lines and therefore appear more similar to L1544 than the starless cores. B335, the prototype of these cores, has been studied in high detail by Zhou et al. (1993) and Choi et al. (1995), who have successfully modeled both the CS and H_2CO emission using the collapse model of a singular isothermal sphere (Shu 1977). Other cores with similar spectral signatures include L1527 (Zhou et al. 1994; Mardones et al. 1994; Myers et al. 1995), IRAS 16293 (Walker et al. 1986; Menten et al. 1987; Zhou 1995), and L1157 (Mardones et al. 1997; Gueth et al. 1997). In all these cases, the self absorption is as deep as in L1544, and the spectrum reaches almost zero intensity at the line center. Statistical studies of the frequency of asymmetries in self-absorbed spectra show that brighter blue peaks tend to prevail toward the youngest stellar objects (Gregersen et al. 1997; Mardones et al. 1997), suggesting that the sense of the peak asymmetry does not result from random kinematics but from a systematic motion. Gravitational infall appears as the most natural explanation.

The similarity of L1544 with some of the infall candidates is not contradicted by the "anomalies" in the CS line shape discussed in § 3.3.1. Reversals of the peak contrast affecting a small fraction of the core have been found in B335 (Kameya et al. 1987), IRAS 16293 (Menten et al. 1987; Zhou 1995), and L1157 (Gregersen et al. 1997). They have been attributed to additional kinematics in the dense gas, like outflows or rotation (Zhou et al. 1993 for B335; Zhou 1995 for IRAS 16293), and, although no kinematical analysis like the one presented in § 3.3.1 has been done for these objects, it seems very likely it would show a similar behavior as in L1544. These perturbations suggest that if the objects are indeed collapsing, the initial conditions may be more complicated than is usually assumed, so further investigation of this problem is of first importance for our understanding of gravitational infall.

From all the above discussion, it seems that L1544 shares more similarities in its physical properties with cores that contain stars (especially Class 0 objects) than with other starless cores. The deep self absorption shows that it has developed a rather massive and thick envelope, and its higher central concentration seems more typical of cores that have undergone (or are presently undergoing) star-forming collapse. All this suggests that the inward motions in L1544 may also be of gravitational origin. We dedicate the next section to discuss this possibility.

4.2. *Interpretation of the Inward Motions*

The inward motions seen in L1544 deserve special attention, because this is the first starless core where such kinematics have been observed. It could be argued that the motions only represent a random velocity pattern that gives a deceiving impression of inward motion. However, the systematics of the pattern, together with the fact that L1544 seems the most centrally concentrated starless core, suggest that the inward motions in L1544 may be related to its star-forming nature. In this section, we compare the observed properties of L1544 with those predicted by several models of early star formation, in particular, ambipolar diffusion and the collapse of a singular isothermal sphere.

Ambipolar diffusion in a self-gravitating cloud is the inward gravitational motion of neutrals against the frictional drag force exerted by collisions with ions tied to a dynamically strong magnetic field. This process has been investigated extensively (e.g., Mestel & Spitzer 1956; Mouschovias & Spitzer 1976; Mouschovias 1977; Shu 1983; Lizano & Shu 1989; Ciolek & Mouschovias 1995, hereafter CM95; Safier, McKee, & Stahler 1997). The numerical simulation of CM95 is perhaps the most detailed available. It considers a self-gravitating cloud of molecules and dust grains, threaded by an initially uniform magnetic field, flattened along the field direction, and ionized by cosmic rays and the interstellar ultraviolet radiation field. According to Figure 7 in CM95, the inward speed of neutrals at a radius of 0.05–0.1 pc (corresponding to our map radius) reaches a maximum of 0.025 km s^{-1} during the quasistatic ambipolar diffusion phase, i.e., up to the time (13 Myr) when the central mass-to-flux ratio becomes equal to the critical value for collapse. The magnetic field is unlikely to lie in the plane of the sky, because then the model cloud would appear highly flattened, in contrast to observations. Assuming that the field direction lies within 45° of the line of sight, the line-of-sight component of the maximum inward neutral speed due to ambipolar diffusion would be <0.02 km s^{-1}. This upper limit on speed is smaller than that inferred from the line profile analysis in § 3.3.1 by up to a factor of 5. Thus it appears unlikely that quasistatic ambipolar diffusion as described by CM95 can match the motions inferred to be present in L1544.

The line profile of HCO^+, shown in Figure 3, also suggests there is no significant drift velocity between neutrals and ions. In the most extreme form of ambipolar diffusion, the magnetic field and the ions would remain fixed in space while the neutrals flowed inward because of gravity. This behavior is predicted in the envelope of the model of Ciolek & Mouschovias (1994), where the ionization is due to cosmic rays alone. Yet the line profile of HCO^+ shows significant infall asymmetry and the largest red-blue ratio of all the lines shown, even though HCO^+ is likely to be the most abundant molecular ion in the dense core. Indeed, most of the line profiles of HCO^+ in a survey of "Class 0" protostars show significant infall asymmetry (Gregersen et al. 1997). It will be useful to quantify the infall speed of HCO^+ through detailed modeling of line profile maps.

The infall of a singular isothermal sphere (Chandrasekhar 1939) has been described by the well-known similarity solution corresponding to "inside-out" collapse (Shu 1977). In this case the infall at each radius is initiated by a rarefaction wave, propagating outward at the sound speed. The time for this wave to achieve infall speed 0.1 km s^{-1} at radius 0.05–0.1 pc is therefore $t = 0.3$–0.5 Myr, assuming sound speed $a = 0.19$ km s^{-1} corresponding to temperature 10 K. But by this time, since the start of infall, one would expect a point source of infrared luminosity

$$L \sim a^6 t/GR_* \,, \tag{1}$$

where R_* is the protostellar radius (e.g., Shu, Adams, & Lizano 1987). Taking $R_* = 3\ R_\odot$ (Stahler 1988), equation (1) yields $L =$ 7–14 $L_\odot$, a luminosity easily detected by *IRAS* at the distance of L1544, where the sensitivity of *IRAS* to a steep spectrum embedded source is about 0.1 $L_\odot$ (Myers et al. 1987). We conclude that L1544 should have produced a detectable protostar by now if its extended infall asymmetry arose from inside-out collapse, whereas no such protostar is known. A way out of this problem is offered by the logotropic model of McLaughlin & Pudritz (1996, 1997), in which a shallower density gradient (r^{-1}) delays the accumulation of the bulk of the star mass to later times. This model, however, predicts that for typical Taurus star masses ($<10\ M_\odot$), a star-forming core will appear as starless for more than 1 Myr, which seems too long given the approximately equal amounts of starless cores and cores with stars in Taurus (Beichman et al. 1986) and that the typical lifetime of a core with star is about 10^5 yr (Myers et al. 1987).

Since neither ambipolar diffusion nor inside-out collapse match the magnitude and spatial extent of the observed infall asymmetry, we now consider the simplest infall system, the collapsing uniform sphere (e.g., Spitzer 1978). The infall speed v at outer radius r of a cold uniform sphere of initial density n_0 and initial radius r_0 can be written

$$v = r_0\left[\frac{8\pi G m n_0}{3}\left(\frac{r_0}{r} - 1\right)\right]^{1/2} , \tag{2}$$

where m is the mean molecular mass and G is the gravitational constant. We adopt $r = 0.06$ pc and $v = 0.08$ km s^{-1} as the mean radius and infall speed associated with the CS zone of infall asymmetry in Figure 7 and choose $n_0 = 3 \times 10^3$ cm^{-3} according to the results from § 3.2.2. Then equation (2) yields $r/r_0 = 0.97$, and equation (13-46) of Spitzer (1978) gives the time since the start of infall as 0.13 Myr. This result implies that the observed size and speed would be consistent with a relatively recent start of infall, so that the cloud had condensed only slightly, by a factor $(r_0/r)^3 = 1.1$. Such a short condensation time, however, is too small to allow an initially uniform sphere to develop the steep density gradient we observe in L1544 (see § 3.2.2). The numerical model of Larson (1969), for example, shows that an initially uniform cloud needs about 0.4 Myr to become centrally concentrated. Thus, collapse from an initially uniform density configuration seems also inconsistent with our observations.

Independently of any infall model, we can use the observed gas parameters to crudely estimate the mass infall rate in L1544. The mass flux for gas of density n, mean molecular mass m, speed v, and area A is simply

$$dM/dt = Amnv \,. \tag{3}$$

We take $n = 3 \times 10^3$ cm^{-3} as discussed above, so our estimate refers to the infall rate in the outer layers of the core (to estimate the inner infall rate, we would need to know the inward velocity near the core center, which does not seem possible with present data). For an area $A = (0.06\mathrm{pc})^2$ and a typical infall speed 0.08 km s^{-1}, equation (3) gives $dM/dt = 2 \times 10^{-7}\ M_\odot\ \mathrm{yr}^{-1}$. This mass flux is lower by an order of magnitude than that expected for the infall of a singular isothermal sphere, and it is probably too low to form a typical Taurus star in a reasonable amount of time (a few 10^5 yr). We can therefore hypothesize that the observed inward motions in L1544 represent precollapse core kinematics or kinematics at the very early stages of collapse.

It is probably premature to interpret these motions further until observations of other starless cores indicate which features of L1544 are peculiar and which are common to other starless cores with infall asymmetry. Also, detailed observations of L1544 in dense gas tracers with self absorptions less deep than those seen in CS and studied here (for example C_3H_2 DCO^+, or N_2H^+) should be made to probe the inward motions closer to the core center. If L1544 is in fact prototypical, our data pose the following dilemma: if the motions we observe represent infall, it appears different from what most theories predict. If is not infall but some other type of motion that precedes star forming collapse, the initial conditions for such process are not of gas at rest, against what is commonly supposed.

5. CONCLUSIONS

We have carried out a multiline study of the starless core L1544 in Taurus, paying special attention to the physical structure and kinematics of its molecular gas. The main conclusions of our work are the following:

1. The L1544 core lies embedded in a more extended, filamentary, molecular cloud, which contains two additional cores. One of them (L1544-E) has already been the place of star formation, as evidenced by the presence of a T Tauri star. The L1544 core, however, appears to be starless.

2. The whole L1544 cloud contains about 30 $M_\odot$ of gas, of which about one-third lies in the three cores. The L1544 core is the most massive and opaque core of the cloud, and toward its center, the optical depth of ^{12}CO (1–0) is about 400. Despite this extreme optical depth, none of the CO (1–0) lines show evidence for self absorption; the gas kinetic temperature in L1544 is either constant or increases slightly toward the outside.

3. In contrast with the CO lines, the optically thick dense gas tracers show strong self absorption, which in the most extreme cases makes the line have almost zero intensity at the center. Most self-absorbed lines have brighter blue peaks caused by the self absorption being slightly redshifted with respect to the emission. This asymmetry in the line indicates that inward motions dominate the gas kinematics along the line of sight. The inward motion appears very extended, as it can be seen in the thickest tracers (CS, H_2CO) all over the core (about 0.2 pc in size).

4. Both emitting and absorbing gases appear centrally concentrated, and a spherical model of a core with constant temperature and a $n \sim r^{-1.5}$ density gradient fits rather well the combination of self-absorbed CS profiles and nonabsorbed CO lines. Different CO and CS isotopes, at different core positions, can be fitted in this way, showing that the self absorption in the dense gas tracers arises from subthermal excitation in the lower density, outer layers of the core.

5. The self-absorbed dense gas tracer lines show changes in the peak contrast over the core. Extremely blue lines appear toward the northwest, while a small region of line reversal (brighter red peak) can be seen toward the south. These changes in the peak contrast indicate that the relative velocity between the front and the back gases varies, reaching values of up to 0.1 km s^{-1} in the most extreme locations. We can satisfactorily reproduce the pattern of line variations with a simple two-layer model in which foreground gas absorbs radiation emitted by a background layer. The absorbing gas has constant velocity over the core, while the emitting gas changes velocity with position and seems to contain two components about 0.2 km s^{-1} apart.

6. The L1544 core seems peculiar among starless cores because of its large optical depth, high degree of concentration, and inward velocity field. In fact, it seems to have more in common with cores containing Class 0 objects, for which there is ample evidence for strongly self-absorbed spectra with brighter blue peaks. We hypothesize that L1544 is a core near the state of forming stars, and that the inward velocity pattern may be related to such a process. We compare the characteristics of L1544 with the predictions from models of ambipolar diffusion and gravitational collapse. Ambipolar diffusion cannot explain the large front-back velocities, while the inside-out collapse model of Shu (1977) cannot explain the simultaneous large extension of the spectral asymmetry and the lack of an embedded central star. We also explore other, less standard infall models, but none of them seems capable of explaining all the features seen in L1544. If this core is in the process of forming stars, our observations suggest that it is doing so in a manner not contemplated by the standard theories of star formation. Our study of L1544 illustrates how little is still known about the physical conditions that precede star formation, and how detailed studies of starless cores are urgently needed.

We thank the staffs of FCRAO, IRAM, and Haystack for help during the observations. We thank Per Friberg for carrying out the JCMT observations and for his generous help and advise during the continuum data reduction. The James Clerk Maxwell Telescope is operated by The Joint Astronomy Centre on behalf of the Particle Physics and Astronomy Research Council of the United Kingdom, the Netherlands Organization for Scientific Research, and the National Research Council of Canada. This research has made use of the SIMBAD database, operated at CDS, Strasbourg, France. R. B. acknowledges partial support from Spanish DGICYT grant PB96-104. P. C. acknowledges support from the ASI-grant ARS-96-66, CNR grant 96/00317, and CNR grant 97.00018.CT02.

REFERENCES

André, P., Ward-Thompson, D., & Motte, F. 1996, A&A, 314, 625
Arquilla, R., & Goldsmith, P. F. 1986, ApJ, 303, 356
Barvainis, R., Ball, J. A., Ingalls, R. P., & Salah, J. E. 1993, PASP, 105, 1134
Beichman, C. A., Myers, P. C., Emerson, J. P., Harris, S., Mathieu, R., Benson, P. J., & Jennings, R. E. 1986, ApJ, 307, 337
Bell, M. B., Avery, L. W., Matthews, H. E., Feldman, P. A., Watson, J. K. G., Madden, S. C., & Irvine, W. M. 1988, ApJ, 326, 924
Benson, P. J., & Myers, P. C. 1983, ApJ, 270, 589
———. 1989, ApJS, 71, 89
Bernes, C. 1979, A&A, 73, 67
Briceño, C., Calvet, N., Gómez, M., Hartmann, L. W., Kenyon, S. J., & Whitney, B. A. 1993, PASP, 105, 686
Butner, H. M., Lada, E. A., & Loren, R. B. 1995, ApJ, 448, 207
Caselli, P., Myers, P. C., & Thaddeus, P. 1995, ApJ, 455, L77
Chandrasekhar, S. 1939, Stellar Structure (New York: Dover)

Cheung, A. C., Chui, M. F., Matsakis, D., Townes, C. H., & Yngvesson, J. 1973, ApJ, 186, L73
Chini, R., Kreysa, E., Mezger, P. G., & Gemund, H.-P. 1984, A&A, 137, 117
Choi, M., Evans, N. J., II, Gregersen, E. M., & Wang, Y. 1995, ApJ, 448, 742
Chu, T. S., Wilson, R. W., England, R. W., Gray, D. A., & Legg, W. E. 1978, Bell Syst. Tech. J., 57, 1257
Ciolek, G. E., & Mouschovias, T. C. 1994, ApJ, 425, 142
———. 1995, ApJ, 454, 194
Clark, F. O. 1991, ApJS, 75, 611
Dieter, N. H. 1973, ApJ, 183, 449
Elias, J. H. 1978, ApJ, 224, 857
Flower, D. R., & Launay, J. M. 1985, MNRAS, 214, 271
Frerking, M. A., Langer, W. D., & Wilson, R. W. 1982, ApJ, 262, 590
Fuente, A., Cernicharo, J., Barcia, A., & Gómez-González, J. 1990, A&A, 231, 151
Fuller, G. A., & Myers, P. C. 1993, ApJ, 418, 273
Gerin, M., Wooten, H. A., Combes, F., Bulanger, F., Peters, W. L., III, Kuiper, T. B. H., Encrenaz, P. J., & Bogey, M. 1987, A&A, 173, L1
Goodman, A. A., Benson, P. J., Fuller, G. A., & Myers, P. C. 1993, ApJ, 406, 528
Gregersen, E. M., Evans, N. J., II, Zhou, S., Choi, M. 1997, ApJ, 484, 256
Gueth, F., Guilloteau, S., Dutrey, A., & Baciller, R. 1997, A&A, 323, 943
Heyer, M. H., Vrba, F. J., Snell, R. L., Schloerb, F. P., Strom, S. E., Goldsmith, P. F., & Strom, K. M. 1987, ApJ, 321, 855
Kameya, O., Hasegawa, T., Hirano, N., Takakubo, K., & Seki, M. 1987, in IAU Symp. 115, Star Forming Regions, ed. M. Peimbert & J. Jugaku (Dordrectht: Reidel), 366
Kuiper, T. B. H., Langer, W. D., & Velusany, T. 1996, ApJ, 468, 761
Ladd, E. F., Adams, F., Casey, S., Davidson, J. A., Fuller, G. A., Harper, D. A., Myers, P. C., & Padman, R. 1991, ApJ, 382, 555
Ladd, E. F., & Heyer, M. 1996, FCRAO Tech. Memo.
Larson, R. B. 1969, MNRAS, 145, 271
Lee, C.-W., et al. 1998, in preparation
Lemme, C., Walmsley, C. M., Wilson, T. L., Muders, D. 1995, A&A, 302, 509
Leung, C. M. 1978, ApJ, 225, 427
Leung, C. M., & Brown, R. L. 1977, ApJ, 214, L73
Lizano, S., & Shu, F. H. 1989, ApJ, 342, 834
Lovas, F. J., & Krupenie, P. H. 1974, J. Phys. Chem. Ref. Data, 3, 245
Lynds, B. T. 1962, ApJS, 7, 1
Mardones, D., Myers, P. C., Caselli, P., & Tafalla, M. 1994, in ASP Conf. Ser. 65, Clouds, Cores, and Low-Mass Stars, ed. D. Clemens & R. Barvainis (San Francisco: ASP), 192
Mardones, D., Myers, P. C., Tafalla, M., Wilner, D. J., Bachiller, R., & Garay, G. 1997, ApJ, 489, 719
McLaughlin, D. E., & Pudritz, R. E. 1996, ApJ, 469, 194
———. 1997, ApJ, 476, 750
Menten, K. M., Serabyn, E., Güsten, R., & Wilson, T. L. 1987, A&A, 177, L57
Mestel, L., & Spitzer, L. 1956, MNRAS, 116, 505
Minn, Y. K., & Greenberg, J. M. 1973, A&A, 22, 13
Mouschovias, T. C. 1977, ApJ, 211, 147
Mouschovias, T. C., & Spitzer, L. 1976, ApJ, 210, 326
Mundy, L. G., Snell, R. L., Evans, N. J., II, Goldsmith, P. F., & Bally, J. 1986, ApJ, 306, 670
Myers, P. C. 1995, in Molecular Clouds and Star Formation, ed. C. Yuan & J. You (Singapore: World Scientific), 47
Myers, P. C., Bachiller, R., Caselli, P., Fuller, G. A., Mardones, D., Tafalla, M., & Wilner, D. J. 1995, ApJ, 449, L65
Myers, P. C., & Benson, P. J. 1983, ApJ, 266, 309
Myers, P. C., Fuller, G. A., Goodman, A. A., & Benson, P. J. 1991, ApJ, 376, 561
Myers, P. C., Fuller, G. A., Mathieu, R. D., Beichman, C. A., Benson, P. J., Schild, R. E., & Emerson, J. P. 1987, ApJ, 319, 340
Myers, P. C., Linke, R. A., & Benson, P. J. 1983, ApJ, 264, 517
Myers, P. C., Mardones, D., Tafalla, M., Williams, J. P., & Wilner, D. J. 1996, ApJ, 465, L133
Parker, N. D. 1988, MNRAS, 235, 139
Pastor, J., Buj, J., Estalella, R., López, R., Anglada, G., & Planesas, P. 1991, A&A, 252, 320
Phillips, T. G., Huggins, P. J., Wannier, P. G., & Scoville, N. Z. 1979, ApJ, 231, 720
Pointer, R. L., & Pickett, H. M. 1995, Appl. Opt., 24, 2335
Preibisch, T., Ossenkopf, V., Yorke, H. W., & Henning, T. 1993, A&A, 279, 577
Ramesh, B., Bronfman, L., & Deguchi, S. 1991, PASJ, 49, 307
Safier, P. N., McKee, C. F., & Stahler, S. W. 1997, ApJ, 485, 660
Sandell, G. 1994, MNRAS, 271, 75
Shu, F. H. 1977, ApJ, 214, 488
———. 1983, ApJ, 273, 202
Shu, F. H., Adams, F. C., & Lizano, S. 1987, AR&A, 25, 23
Snell, R. L. 1981, ApJS, 45, 121
Spitzer, L. 1978, Physical Processes in the Interstellar Medium (New York: Wiley)
Stahler, S. W. 1988, ApJ, 332, 804
Tafalla, M., & Myers, P. C. 1997, ApJ, 491, 653
Tolmachev, A. M. 1995, Astron. Lett., 21, 32
Turner, B. E., Chan, K.-W., Green, S., & Lubowich, D. A. 1992, ApJ, 399, 114
Turner, B. E., & Sears, T. J. 1989, ApJ, 340, 900
Turner, B. E., Tsuji, T., Bally, J., Guelin, M., & Cernicharo, J. 1990, ApJ, 365, 569
Ungerechts, H., & Thaddeus, P. 1987, ApJS, 63, 645
Ungerechts, H., Walmsley, C. M., & Winnewisser, G. 1982, A&A, 111, 339
Walker, C. K., Lada, C. J., Young, E. T., Maloney, P. R., & Wilking, B. A. 1986, ApJ, 449, L65
Walker, C. K., Narayanan, G., & Boss, A. P. 1994, ApJ, 431, 767
Ward-Thompson, D., Scott, P. F., Hills, R. E., & André, P. 1994, MNRAS, 268, 276
White, R. E. 1977, ApJ, 211, 744
Wild, W. 1995, The 30 m Manual: A Handbook for the 30 m Telescope, IRAM Tech. Rep. 377/95
Wood, D. O. S., Myers, P. C., & Daugherty, D. A. 1994, ApJS, 95, 457
Zhou, S. 1995, ApJ, 442, 685
Zhou, S., Evans, N. J., II, Kömpe, C., & Walmsley, C. M. 1993, ApJ, 404, 232
Zhou, S., Wu, Y., Evans, N. J., II, Fuller, G., & Myers, P. C. 1989, ApJ, 346, 168